Electrospun quad-axial nanofibers for controlled and sustained drug delivery

Xindan Zhang [a,b], Cheng Chi [a,b], Junjie Chen [a], Xiaodi Zhang [a,b], Min Gong [a,b], Xing Wang [a], Junhao Yan [c], Rui Shi [d,*], Liqun Zhang [a,b], Jiajia Xue [a,b,*]

[a] Beijing Laboratory of Biomedical Materials, Beijing University of Chemical Technology, Beijing 100029, PR China
[b] State Key Laboratory of Organic-Inorganic Composites, Beijing University of Chemical Technology, Beijing 100029, PR China
[c] Department of Anatomy and Histology, School of Basic Medical Sciences, Peking University, Beijing 100191, PR China
[d] Institute of Traumatology and Orthoaedics, Beijing Jishuitan Hospital, Beijing 100035, PR China

A B S T R A C T

It is of great importance and a major challenge to achieve a controlled delivery of specific types of active ingredients for tissue regeneration. Herein, we report a system comprised of electrospun quad-axial nanofibers fabricated by quadriaxial electrospinning, with the material components in the different layers can be well regulated. The quad-axial nanofibers allow the regulation of the type of materials in different layers as well as the manipulation of the location of drug in the nanofibers, representing a promising controlled drug release system. In one typical example, we apply polycaprolactone to construct both the outermost and second innermost layers while gelatin to construct both the second outermost and innermost layers. The nanofibers with a cleared four-layered nanostructure are confirmed by morphological evaluations. Moxifloxacin, a type of antibacterial drug serving as a model of therapeutic payload, is encapsulated in the different layers of the nanofibers, realizing an effective control of the drug delivery. In addition, the efficacy for drug delivery with the use of quad-axial nanofibers is superior to that of core-sheath and blended nanofibers. This quadriaxial electrospinning technique can be widely used for the co-delivery of factor cocktails in a designed sequence, which will show great potential for tissue engineering.

© 2021 The Author(s). Published by Elsevier Ltd. This is an open access article under the CC BY-NC-ND license (http://creativecommons.org/licenses/by-nc-nd/4.0/).

1. Introduction

The regeneration of defected tissue is a complex process, which can be usually divided into several stages [1]. For example, the healing process of bone defects consists of four stages: hematoma formation (including inflammation), fibrogenic callus formation, osseous callus formation, and callus reconstruction or remodeling [2]. In general, during this long rehabilitation process, different types of drugs or growth factors are required for the typical stages due to the specific emphases during the healing process [3]. For instance, controlled co-delivery of bone morphogenetic protein-2 (BMP-2) and connective tissue growth factor could allow the two factors working together to stimulate the activity of osteoblasts and promote bone formation [4]. Sustained delivery of vascular endotheliar growth factor (VEGF) and collagen from hyaluronan-poly(*L*-lactide) core-sheath nanofibers also indicated the improvement of bone regeneration [5]. Therefore, it is desirable to fabricate a scaffold capable of delivering specific types of growth factors or drugs during the different stages to improve the efficacy of tissue regeneration.

Among various methods for producing the scaffold, one promising strategy is based on electrospinning, through which drugs can be introduced into the nanofibrous scaffold and their release in different time ranges can be controlled [6]. Because of their capability of mimicking the structure and component of the extracellular matrix (ECM) in a certain extent, electrospun nanofibers have gained widespread interests for drug delivery and tissue engineering [7–11]. Various types of materials have been utilized for electrospinning to fabricate nanofiber platforms for regulating cell adhesion, proliferation, and differentiation [12,13]. The morphology, physical properties, and biodegradability of electrospun nanofibers, as well as drug release from the nanofibers can be adjusted through the optimization of the fabrication parameters [14–16]. Typically, the drug release rate can be controlled through diffusion or accompanied by polymer degradation [17–20]. For example, a mixture of three types of active ingredients (*i.e.*, BMP-2, VEGF and mineralization drug Ca-P) were integrated with polymers to

produce electrospun nanofiber scaffolds [18,19]. In the case of retaining their biological activity, the three drugs can be released simultaneously. However, the use of hybrid electrospinning methods cannot achieve the orderly release of drugs on demand. Therefore, it is of great importance to prepare a nanofiber scaffold for providing the specific type of drug at the targeted therapeutic stage, which remains to be a challenge.

Tackling these challenges, co-axial electrospinning has been investigated to prepare co-axial nanofibers [21]. Through a careful design of the matrix materials and the protective effect of the sheath layer, two different types of drugs can be separately encapsulated in the core and sheath layers and then released at different rates [22]. In one study, acyclovir was loaded in the sheath and bovine serum albumin in the core, respectively, of co-axial nanofibers, and a controlled release of the two types of drugs was achieved [23]. A similar result was also observed by integrating ampicillin in the core and bovine serum albumin in the sheath of co-axial nanofibers [24,25]. The core-sheath structure not only enhances drug encapsulation but also accomplishes controlled and sustained drug delivery [26–28].

Co-axial electrospinning of multiple-fluids has been further developed to improve the versatility and controllability of the system [29–31]. For example, tri-axial electrospinning is used to fabricate tri-axial nanofibers composed of different biodegradable polymers in each layer, enabling their application for regulating the delivery of typical payloads [32]. In one study, tri-axial nanofibers were developed by triaxial electrospinning, with gelatin used as both the sheath and core layers while polycaprolactone (PCL) as the middle layer [7]. By regulating the matrix materials of the triaxial nanofibers, a controlled release of ibuprofen and ketoprofen was realized [30]. In order to endow the nanofibers with a more stratified drug release ability, quadriaxial electrospinning has been explored recently. Quad-axial fibers made of four different biocompatible polymers, *i.e.*, polyethylene glycol, poly(lactic-*co*-glycolic acid), PCL, and polymethylsilsesquioxane, in different layers were fabricated [33]. The incorporation of different dyes within the system confirmed the fabrication of the quad-axial core-sheath structure. To this end, quad-axial nanofibers show great promise in regulating the release of payloads, and it is of great importance to investigate their capability for controlling the release of therapeutic drugs.

Numerous natural and synthetic polymers have been investigated to fabricate nanofiber scaffolds for drug delivery and tissue engineering. PCL, a semi-crystalline biodegradable polyester, has been intensively used in tissue engineering because of its excellent mechanical properties [34,35]. However, despite its good mechanical strength, PCL shows strong hydrophobicity, poor cell attachment, slow biodegradation rate and lack of bioactive functions [36]. Co-electrospinning of PCL with other bioactive materials such as gelatin can increase the biocompatibility of the obtained nanofibers and promote the efficacy of the fabricated scaffolds for tissue regeneration [37]. Gelatin has a unique advantage in controlled drug delivery owing to its attractive characteristics, such as good biocompatibility and biodegradability [38]. Electrospun nanofibers made of the hybrid of PCL and gelatin, with adjustable biodegradation rates and drug delivery profiles, have been successfully used for drug delivery and tissue regeneration [39].

In the present work, we applied quadriaxial electrospinning to form a compound jet made of four-layered fluids in a concentric manner, and then we investigated the generation of quad-axial nanofibers by varying the material component of the four different layers (Fig. 1). Due to its long half-life and less adverse reaction, without developing drug resistance, moxifloxacin (MXF), a broad-spectrum antibacterial quinolone drug, is often applied for clinical treatment of infection in skin and soft tissues [40]. Therefore, MXF serving as a therapeutic factor was then loaded in the different

positions of the nanofibers [41]. Afterwards, we investigated the release behavior of the drug from the quad-axial nanofibers. As a comparison, the drug was also loaded in the nanofibers made of a mixture of PCL and gelatin, or encapsulated in the core of PCL-gelatin core-sheath nanofibers, which were fabricated by single-spinneret or core-axial electrospinning, respectively. This work aims to provide valuable information for the development of a multifunctional system based on multilayered coaxial nanofibers for controlled drug delivery.

2. Materials and methods

2.1. Materials

PCL ($M_n \approx 80$ kDa), dimethyl sulfoxide (DMSO), and 3-(4,5-dimethylthiazol-2-yl)-2,5-diphenyl tetrazolium bromide (MTT) were all obtained from Sigma-Aldrich (USA). Gelatin (Type B) was obtained from Rousselot (France). MXF was purchased from Shanghai Macklin Biochemical Technology Co., Ltd. (China). Cell Counting Kit-8 (CCK-8), tryptone, yeast extract, nutrient agar, dulbecco's modified eagle medium (DMEM), fetal bovine serum (FBS), and phosphate buffer saline (PBS, PH = 7.4) were purchased from Hyclone (USA). Trifluoroethanol (TFE) was purchased from Aladdin. L929 mouse fibroblasts cells were kindly donated by Jishuitan Hospital. *Staphylococcus aureus* was purchased from China General Microbiological Culture Collection Center.

2.2. Fabrication of quadriaxial electrospun nanofibers

A quad-axial needle consisting of four concentric hollow needles, with an inner diameter of 0.40 1.07, 1.90 and 2.54 mm, respectively, was used as the spinneret during quadriaxial electrospinning to generate a quad-axially electrified jet. Four syringe pumps were used to separately drive four fluids into the outermost, second outermost, second innermost, and innermost needles at controllable flow rates. As shown in Fig. 1, when these fluids meet at the exit end of the quadriaxial needle, the outer fluids will wrap around the inner fluids to form a compound Taylor cone in the presence of an external electric field, followed by the ejection of a quadriaxial jet. Finally, quad-axial nanofibers with distinct compositions will be obtained.

In our typical experiment, PCL pellets and gelatin were separately dissolved in TFE to obtain homogeneous electrospinning solutions at a concentration of 6 wt%. The PCL solution was applied as the outermost and second innermost fluids, and gelatin solution was applied as the second outermost and innermost fluids, respectively. In order to obtain the quad-axial nanofibers, we optimized the parameters for the quadriaxial electrospinning by a large number of pre-experimental explorations, and set the fluid speeds as 1.3, 0.3, 0.3, and 0.1 mL/h, respectively, from the outermost to the innermost layers. In this case, in the generated quad-axial nanofibers with multiple-layered structure, the outermost and second innermost layers were made of PCL, which were labeled as PCL-out and PCL-in, respectively; while the second outermost and innermost layers were made of gelatin, which were labeled as Gel-out and Gel-in, respectively. To investigate the influence of the loading position of the drug in the nanofibers on their release profile, we separately encapsulated MXF in the four different layers of the nanofibers by dissolving MXF in the corresponding electrospinning solutions at a mass ratio of 3 wt% to the corresponding polymer components. Four different types of drug-loaded quad-axial nanofibers were thus generated.

As control groups, co-axial and blended nanofibers were also fabricated for drug release. For coaxial electrospinning, PCL pellets were dissolved in TFE at a concentration of 6 wt% and applied as
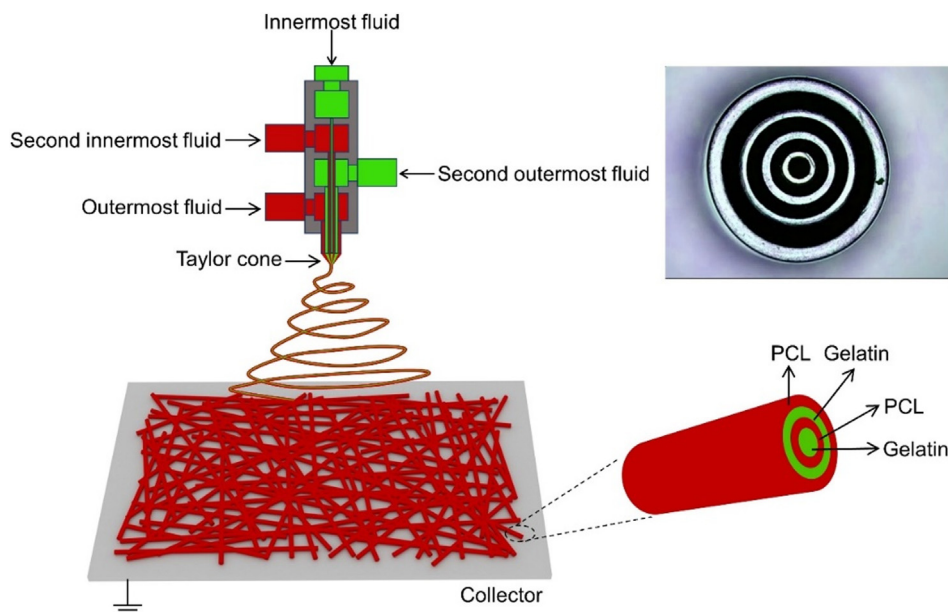
Fig. 1. Schematic diagram of quadriaxial electrospinning. The inset in the upper right shows a photograph of the concentric spinneret.

the outer fluid. Gelatin was dissolved in TFE at a concentration of 6 wt%, and then MXF, at a mass ratio of 3 wt% to gelatin, was added to the solution. After stirring for 24 h, a homogeneous solution was obtained and applied as the inner fluid. The outer and inner fluids were simultaneously pumped out through a coaxial spinneret at a speed of 1.6 and 0.4 mL/h, respectively, to produce the core-sheath PCL-gelatin nanofibers. For blending electrospinning, PCL and gelatin (at a mass ratio of 4:1) were simultaneously dissolved in TFE at a concentration of 6 wt%, and then MXF, at a mass ratio of 3 wt% to the polymer component, was added to the solution. After electrospinning with the use of hollow needle, blended nanofibers made of the mixture of PCL and gelatin and encapsulated with the drug were generated. To better distinguish the different samples and evaluate the influence of the fiber structure on the drug release, the blended, core-sheath, and quad-axial (when MXF was loaded in the innermost gelatin layer) nanofibers were named as 1-NF, 2-NF, and 4-NF, respectively.

2.3. Morphology characterization of the electrospun nanofiber membranes

The morphology of the nanofibers was observed under the scanning electron microscope (S4800, Hitachi, Japan) at a voltage of 5 kV. The average diameter of the nanofibers was measured using the Image J software from 200 nanofibers at random locations of the scanning electron microscopy (SEM) images [42].

2.4. Internal structure of the electrospun nanofibers

During quad-axial electrospinning, a carbon coated copper grid was placed on the top of the collector, and the nanofibers were deposited onto the copper grid for several seconds. Afterwards, the internal structure of the nanofibers was observed under a transmission electron microscope (H-800, Hitachi, Japan).

2.5. In vitro biodegradation of the electrospun nanofiber membranes

The nanofiber membranes were cut into circles with 2 cm in diameter, accurately weighed, and then soaked in 5 mL of PBS solution in the wells of a 12-well plate at 37°C. At predetermined time

points, the samples were washed with deionized water for three times, dried at room temperature until no mass change, and then weighed. The weights of the samples were plotted against time to obtain the degradation profile of the nanofiber membranes [42].

2.6. Drug release profile of the electrospun nanofiber membranes

The drug release profiles of different types of electrospun nanofiber membranes were tested by soaking the samples in PBS solution at 37°C. At predetermined time points, the solutions were collected for UV–vis characterization and replaced with fresh PBS to maintain the sink condition. The concentration of released drug was determined by a UV–vis spectrophotometer (UV-1700, Macy instrument, China) at 296 nm. The percentages of released drug at typical points of time were calculated based on the weight of the drug incorporated in the nanofiber membranes. Triplicate samples were used for each group.

2.7. In vitro biocompatibility of the electrospun nanofiber membranes

L929 mouse fibroblasts were used as the model cells to test the *in vitro* biocompatibility of the different types of nanofiber membranes. The cytotoxicity of each type of membrane was evaluated by MTT assay following the below steps [43]. The sample was cut into a disc at a diameter of 3 cm, sterilized, and then soaked in 5 mL DMEM. After 24 h, the culture medium was retrieved, filtrated, and then mixed with FBS to obtain the extraction solution of the sample. Afterwards, the cells were resuspended in 100 μL of the extraction at a density of 1×10^4 cells/mL and then added to the well of a 96-well plate. After incubation for 24, 48, and 72 h in a cell incubator at 37°C under 5% CO_2 atmosphere, respectively, the morphologies of the cells were observed under an inverted microscope. To characterize the relative growth rate (RGR) of the cells after incubation in the extraction solutions of different samples, 20 μL of MTT solution was added to each well followed by incubation for another 4 h. Afterwards, the solution in each well was replaced by 200 μL DMSO. The optical density (O. D.) of the obtained solution at 630 nm was measured using a microplate reader. The cells were also incubated in the cell culture medium and in DMSO, respectively, to serve as the blank control

group and the negative group. Triplicate samples were used for each group.

The RGR was calculated by using equation (1):

$$RGR(\%) = \frac{OD_{test} - OD_0}{OD_{control} - OD_0} \times 100\%. \tag{1}$$

Herein, OD_{test}, $OD_{control}$ and OD_0 represent the optical densities of the experimental group, negative control, and blank control, respectively.

The viabilities of L929 cells proliferated on the different types of nanofiber membranes were evaluated by CCK-8 assay [44–45]. The membranes were cut into circles at a diameter of 3 cm, sterilized, and then fixed in the well of a 24-well plate by Cell-Crown™. L929 cells were resuspended in DMEM supplemented with 10% FBS and antibiotics at a density of 4.0×10^4 cells/mL. Then, the mixture of cell culture medium (900 μL) and cell suspension (100 μL) was plated onto the sample, and the cells were incubated at 37℃ under 5% CO_2 atmosphere. The cell culture medium was changed every two days. At days 1, 3, 5, and 7, CCK-8 (100 μL) solution was added to the medium of each well and incubated for 4 h. Then, the culture medium was transferred into a 96-well plate for O.D. measurements at 450 nm. The cells incubated on the tissue culture plate was set as the blank control group. To observe the morphologies of the cells cultured on the different types of nanofiber membranes, the cells were washed with PBS for three times, fixed with 3% glutaraldehyde solution for 2 h, and dehydrated through a series of graded ethanol solutions. After totally dried out, the morphologies of the cells on the membranes were characterized using SEM.

2.8. In vitro antibacterial function of the electrospun nanofiber membranes

The antibacterial activities of the different types of nanofiber membranes against *Staphylococcus aureus* (*S. aureus*), a typical type of gram-positive bacterium, were determined by the following method [46]. Briefly, the suspension of the bacteria was inoculated into Luria-Bertani (LB) medium and then incubated at 37°C. After 24 h, isolated bacterial colonies were resuspended until the turbidity was compatible with 1.0 Mac Farland. Afterwards, 100 μL bacterial suspension was spread onto the agar plate in a culture dish, and then square sample with a width of 1.0 cm was placed on the top. Triplicate samples were evenly distributed and placed on the same petri dish. After incubation for different periods of time at 37°C, photos were taken, and the diameters of the inhibition zones were measured [45]. Triplicate samples were used for each group.

2.9. Statistical analysis

All quantitative data were expressed as mean ± standard deviation (SD). Statistical analyses were performed using the OriginPro 8 software (Hampton, OriginLab).

3. Results and discussion

3.1. Morphologies of the electrospun nanofiber membranes

Nanofiber membranes composed of blended, core-sheath, and quad-axial nanofibers were fabricated using 1 single hollow needle (1-NF), co-axial needle (2-NF), and quad-axial needle (4-NF), respectively, and their morphologies are reflected by the SEM images, as shown in Fig. 2a-c. For all the three types of the nanofiber membranes, the nanofibers exhibited a smooth surface with no beads formed and were deposited randomly with interconnected pores. The average diameters of the nanofibers for the 1-NF, 2-

NF, and 4-NF membranes were 440 ± 170, 650 ± 210, and 780 ± 110 nm, respectively, indicating the increase of the diameter with the layers in the individual nanofiber. It is rather remarkable that the diameter of the nanofibers and the thickness of the different layers can also be changed by modifying the flow rates of the fluids. The porous structure provided the nanofiber membranes with both permeability and flexibility, which are desirable for the competent drug release for tissue regeneration.

To ensure a robust and reproducible generation of quad-axial nanofibers with four layers, a high co-axiality of the quad-axial needle is the preliminary request. In addition, the four fluids should have sufficient viscosities to keep the jet continuous. The miscibility among the four fluids is also an important factor, as it will be difficult to generate a quadriaxial jet from four fluids that are rapidly miscible. The different parts of the jet should be stretched simultaneously to generate four-layered nanofibers by avoiding possible mixing or inversion of the four fluids. The four fluids should also have similar dielectric properties to ensure a similar electrical force. In addition, the flow rates of the fluids need to be carefully adjusted to ensure that the inner fluids will be fully wrapped by the outer fluids. Under the premise of meeting these technical requirements, we obtained the quad-axial nanofibers through quadriaxial electrospinning. Fig. 2d depicted a transmission electron microscopy (TEM) image of the generated nanofibers. It exhibited a clear four-layered structure, with the PCL layer showed a dark gray color and the gelatin layer showed a light gray color. From the innermost core to the outermost sheath, the four layers were made of gelatin, PCL, gelatin, and PCL, respectively. These differences in color could be attributed to the different matrix in each layer. To further confirm the quad-axial structure of the nanofibers, we also added phalloidin (yellow) and Rhodamine B (red) to the gelatin and PCL components, respectively, by adding the dyes to the corresponding polymer solutions for electrospinning. From the fluorescence micrographs of the nanofibers in Fig. 2, e and f, an obvious four-layered structure, which were marked as green and red from innermost to outermost alternately, were observed. Compared with the electrospun core-sheath nanofibers, the addition of the third and fourth layers were realized.

3.2. In vitro biodegradation of the nanofiber membranes

It is of great importance that the implanted nanofiber membranes can synchronize their degradation and tissue regeneration to minimize long-term interference [47,48]. Fig. 3 shows the mass losses of the different nanofiber membranes within 7 days. The hydrophilic natural polymer gelatin hydrolysis rapidly in PBS while PCL takes about two years to fully degrade [49]. Due to the degradation of gelatin, all the three types of nanofiber membranes showed an obvious mass loss within the first week. The nanofiber membranes composed of 2-NF exhibited the fastest degradation rate, which could be attributed to the quick dissolution of the hydrophilic gelatin in the core component and the percent difference of the gelatin component in the nanofibers. The percentage of mass loss of the 4-NF membrane was similar to that of 2-NF, which could be attributed to the dissolution of the two layers made of gelatin. Even though under the protection of the two PCL-layers, when the surrounding fluid contacted with gelatin to make it starting dissolve, the dissolution of gelatin would be accelerated. For the membrane made of blended nanofibers, the mass loss was also attributed to the degradation of gelatin, during which the gelatin was mixed with PCL component, leading to a slower degradation rate.
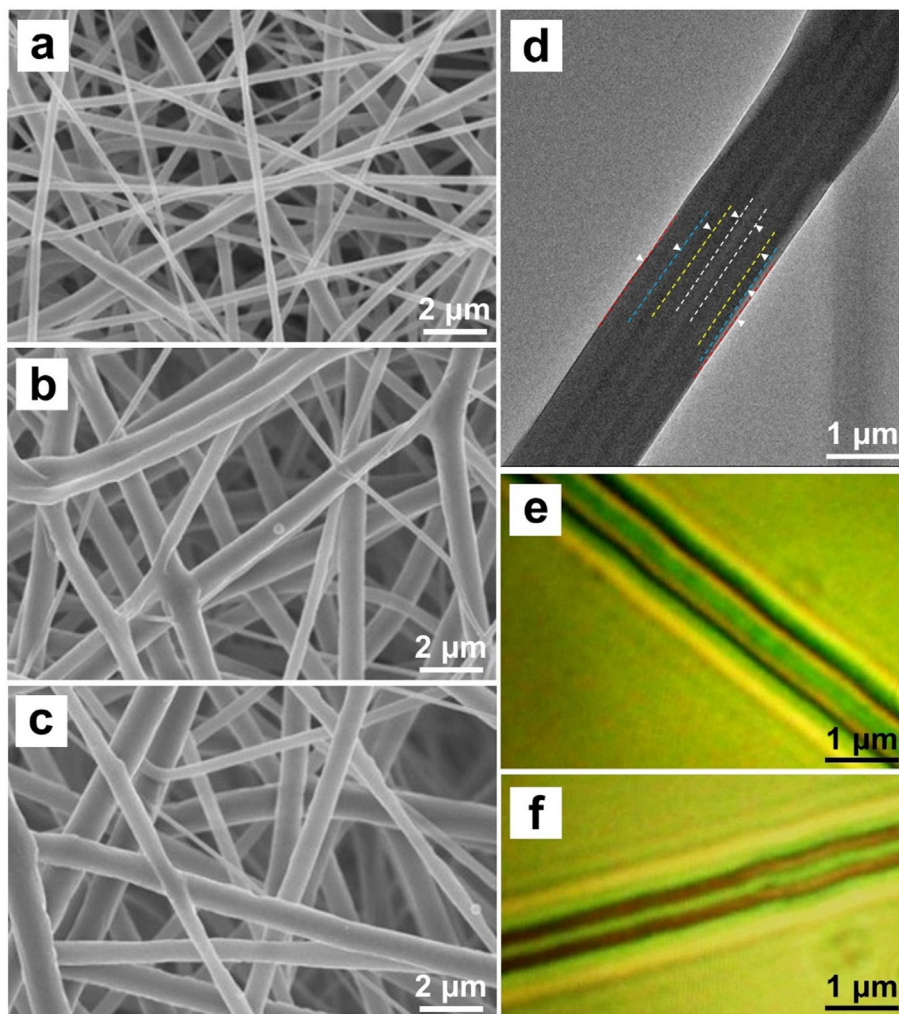
Fig. 2. SEM images of the nanofiber membranes composed of (a) 1-NF, (b) 2-NF, and (c) 4-NF, respectively. (d) TEM image and (e-f) optical micrographs of a quad-axial nanofiber.
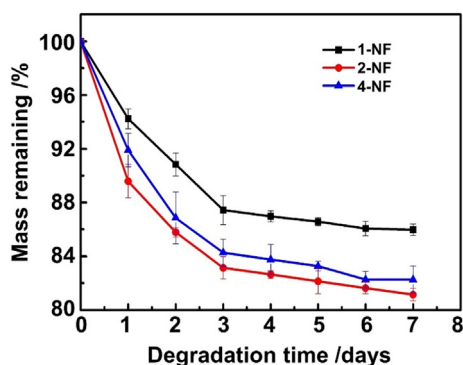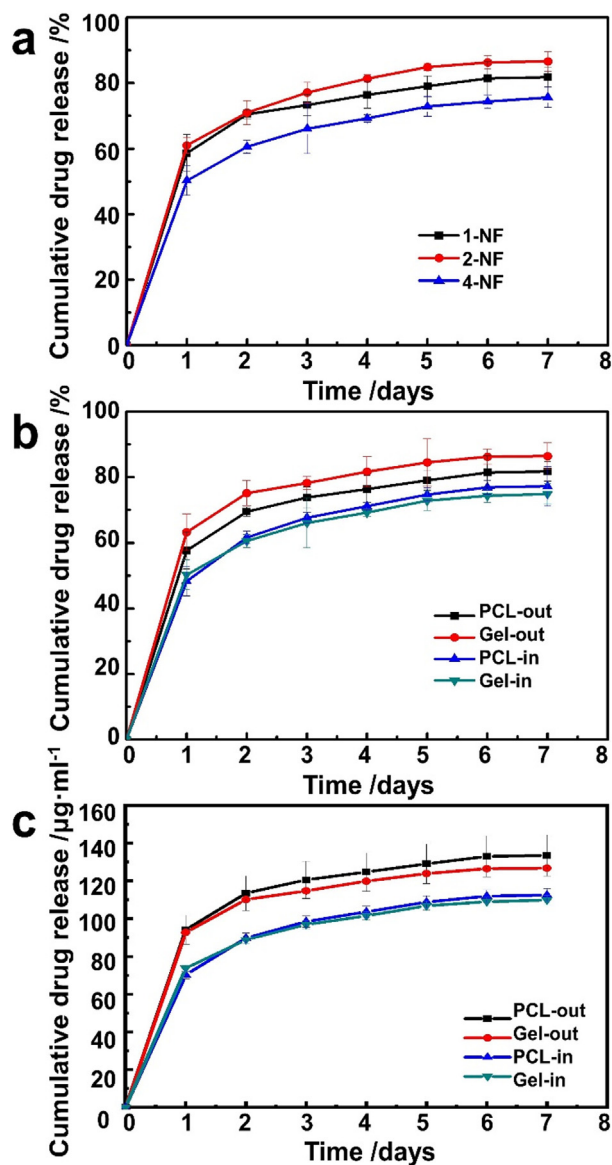

Fig. 3. Mass loss of the different types of nanofiber membranes after *in vitro* degradation for 7 days.

3.3. Drug release profiles of the electrospun nanofiber membranes

The drug release profile of a scaffold greatly affects its efficacy for disease treatment and tissue regeneration. Securing an appropriate drug release profile is essential for the nanofiber membranes to be used in an *in vivo* application. The drug release profiles of the three types of nanofiber membranes are presented in Fig. 4. For all the three types of nanofiber membranes, a burst release of about 50–60% of drug was observed. Afterwards, the drug was released at a slower rate. In addition to diffusion of the drug component from the nanofibers into the surrounding environment, polymer degradation also contributes to the drug release [49]. When the percentage of drug released from the nanofiber membrane was calculated to measure the degradation rate, drug release accompanied by gelatin degradation illustrated the sorting of drug release rates herein. From Fig. 4a, the rate of drug release from the 4-NF membrane was the slowest, which could be attributed to that the drug was loaded in the innermost layer of the nanofibers and protected by the three outer layers. For the nanofiber membranes made of core-sheath nanofibers and blended nanofibers, they did not show significant differences for the drug release rates. From the degradation experiments, the degradation rate of 2-NF was quicker than that of 1-NF due to the core-sheath structure and the dissolution of the gelatin layer. At the same time, however, the sheath layer in a core-sheath nanofiber could retard the release of drug from the inner core. Therefore, these two reasons led to the results of the non-significant difference in their drug release rates.

In order to evaluate the influence of the drug loading position in the nanofibers on the release profile, we separately loaded the drug in the four different layers of the quad-axial nanofibers to fabricate different types of nanofiber membranes. The drug was loaded in the innermost gelatin, inner PCL, outer gelatin, and outermost

Fig. 4. The cumulatively released percentage of drug from the different types of nanofiber membranes composed of blended (1-NF), core-sheath (2-NF), and quad-axial (4-NF) nanofibers, respectively. The cumulatively released (b) percentage and (c) concentration of drug when loaded in the different position of the nanofiber membranes.

PCL layers, respectively, and the obtained nanofiber membranes were labeled as Gel-in, PCL-in, Gel-out, and PCL-out. The cumulatively released percentages and concentrations of the drug are presented in Fig. 4, b and c, respectively. For all the nanofiber membranes, the curves of the drug release profiles exhibited a downtrend of the slope of the tangent line, indicating a sustained drug release performance of 4-NF. Moreover, when drug was loaded in the innermost layer, the slope of the tangent line reached a minimum value, which proved that the slowest drug release rate was obtained when the drug was loaded in the Gel-in layer, providing valuable information for fabricating controlled drug release system based on multilayered nanofibers. From the curve indicating the cumulatively released percentage of the drug, we found that the release rate of the drug loaded in the two inner layers made of gelatin and PCL was the slowest, while the release rate when the drug was loaded in the outermost PCL was the fastest. The degradation of gelatin and the diffusion of drug happened

simultaneously for the two groups of loading drug in the gelatin layer. Defects in the outermost PCL layer and exposure of the inner gelatin layer both led to the quicker release of the drug from Gel-out than PCL-out, for the degradation rate of gelatin far outweighed that of PCL. Regarding the Gel-in and PCL-in, a slower drug release rate could be attributed to the outer layers' protection, under which they showed a delayed drug release profile compared to Gel-out and PCL-out. The third layer's surrounding accounted for the slowest drug release rate of the Gel-in.

3.4. In vitro biocompatibility of electrospun nanofiber membranes

The good biocompatibility of a scaffold is one of the basic requirements for its *in vivo* application. As shown in Fig. 5a, all the nanofiber membranes showed no cytotoxicity towards L929 cells, with RGR > 90% after incubation in the extracted media of the membranes for 24 h. After incubation for 48 h and 72 h, the RGR of the cells still exceeded 80%, indicating that the three types of nanofiber membranes showed no cytotoxicity towards L929 cells. As shown in Fig. 5b, L929 cells exhibited healthy morphologies as spindle shapes, which further proofed that the electrospun nanofiber membranes did not adversely affect the growth of L929 cells. To this end, the cytotoxicity results indicated the safety of using the quad-axial electrospun nanofiber membranes as a potential drug delivery system *in vivo*.

Attachment and proliferation are the first phase in cell-material interactions and have significant influence on cell proliferation rate and morphology [45]. As shown in Fig. 6a, all the nanofiber membranes supported the proliferation of cells, on account of the increasing number of cells and the consistently good growing condition of cells. In the first 3 days, cells exhibited a preference to interact with the tissue culture plate (TCP). After incubation for 7 days, the proliferation of cells on the nanofiber membranes showed no significant differences with that on TCP, indicating the good biocompatibility of the drug loaded nanofiber membranes.

Fig. 6b shows the SEM images of the cells after incubation on the different types of nanofiber membranes for 5 days. The cells grew healthily and could spread on the surface of the membranes without infiltrating into the thickness direction owing to the small pore sizes of the membrane. The L929 cells tended to achieve high degree of confluency on the surface of the nanofiber membranes. Additionally, they were observed to have fibroblasts–filopodia and lamellipodia, which are related to the cell motility, indicating the adhesion and migration of cells on the nanofiber membranes. All the evidence indicated that the different types of nanofiber membranes had no adverse effect on the cell morphology and proliferation. To conclude, the results of *in vitro* biocompatibility experiments confirmed that even with the use of organic solvent during the electrospinning process and the encapsulation of drug, the electrospun nanofibers with different nano-structures had no negative influence on the cell morphology, viability, and proliferation.

3.5. In vitro antibacterial capability of the electrospun nanofiber membranes

The antibacterial capabilities of the nanofiber membranes were evaluated by bacterial inhibition experiments. The growth of *S. aureus* could be visualized directly from the plates to assess the antibacterial activity. In our previous work, no inhibition zone for *S. aureus* had been observed around the drug-free core-sheath PCL-gelatin nanofiber membranes [46]. Herein, as shown in Fig. 7, the inhibition zone on the plate was visualized evidently in the three types of the nanofiber membranes at the initial stage of experiment. After incubation the bacteria with the nanofiber
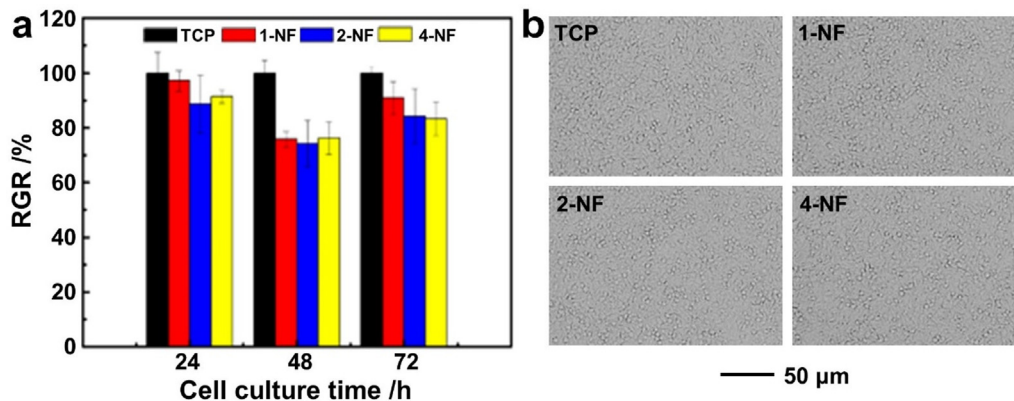
Fig. 5. The *in vitro* cytotoxicity evaluation of the electrospun nanofiber membranes by incubating L929 cells in the extracted solutions of the samples. (a) RGR of L929 cells after incubation for different time, and (b) microscope images of L929 cells after incubation for 72 h.
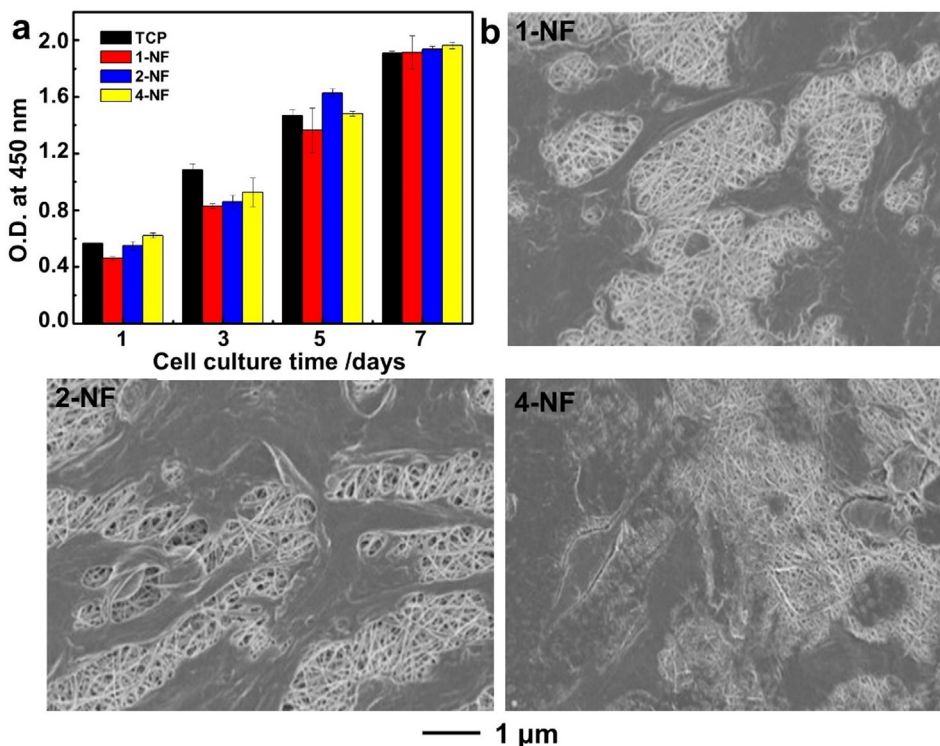

Fig. 6. (a) O.D. values of L929 cells after incubation on the TCP and different types of electrospun nanofiber membranes for different periods of time. (b) SEM images of L929 cells after proliferated on different types of membranes for 5 days.

membranes for one day, the diameters of the inhibition zone for the groups of 1-NF, 2-NF and 4-NF were 23.3, 23.3, and 20.0 mm, respectively. After incubation for 7 days, the inhibition zone grew and the diameters reached 26.7, 28.3, and 23.3 mm, respectively, indicating a long-term antibacterial activity for all the drug loaded electrospun nanofiber membranes.

As shown in the drug release experiments, the drug release rate of 2-NF was quicker than that of 1-NF, meanwhile, the 4-NF presented the slowest and sustained drug release rate due to the four-layered core-sheath structure. As shown in the figures, the size of the inhibition zone of 2-NF remained to be the largest through the whole process of the antibacterial experiment, while the 4-NF sustained to possess the smallest diameter, which

demonstrated that the 4-NF would be released more persistently to maintain long term antibacterial effect.

The sizes of inhibition diameters varied for the different drug release rates, and consequently showed various antibacterial activity of different samples. Herein, drugs loaded in the nanofiber membranes were all sufficient to resist bacterial growth within 7 days. Hence, similar antibacterial activity was found during 7 days, indicating that the three groups of nanofiber membranes all had equally durable antibacterial capabilities. Additionally, owing to the diffusion of MXF into the agar, the nanofiber membranes could inhibit bacterial growth in an area much larger than the membrane size. All these evidences indicated that the drug-loaded nanofiber membranes could inhibit the colonization of bacteria.
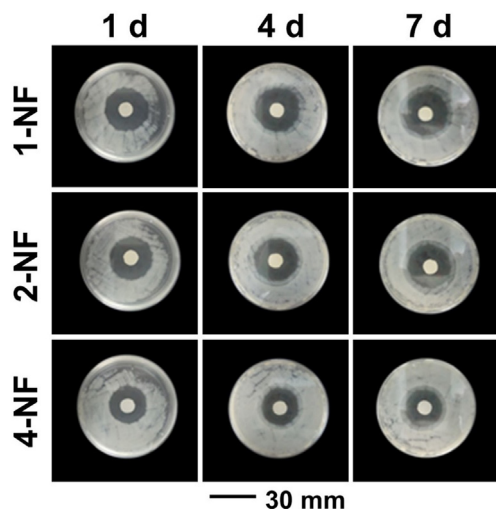
Fig. 7. Optical images of the inhibition zones around the electrospun nanofiber membranes against *S. aureus* after incubation for 1, 4, and 7 days, respectively.

4. Conclusions

In this study, we fabricated quad-axial nanofibers by quadriaxial electrospinning to develop a controlled and sustained drug release system. The components of the four different layers of the quad-axial nanofibers could be regulated by changing the injected fluids. Both the degradation and drug release profiles of the nanofiber membranes were affected by the nano-structure of the nanofibers. The quad-axial nanofibers prolonged the period of drug release effectively in comparison with core-sheath nanofibers and blended nanofibers. In addition, the position of the drug loaded in the four different layers of the quad-axial nanofibers also showed influence on the drug release rate, indicating the potential of applying this system for the sequential release of multiple therapeutic components. The *in vitro* cytotoxicity and proliferation experiments indicated that the nanofiber membranes had no adverse effect on cell morphology and proliferation, suggesting their good biocompatibility as drug release systems. The *in vitro* antibacterial evaluation proved the excellent antibacterial function of the quad-axial nanofiber membranes loaded with antibacterial drugs. The increasing sizes of inhibition zones further demonstrated the release of antibacterial drug from the nanofiber membranes. The generated nanofiber membranes composed of quad-axial nanofibers can be broadly applied for therapeutic approaches in which precise and effective drug delivery are necessary.

Declaration of Competing Interest

The authors declare that they have no known competing financial interests or personal relationships that could have appeared to influence the work reported in this paper.

Acknowledgments

References

[1] K.T. Shalumon, G.J. Lai, C.H. Chen, J.P. Chen, Modulation of bone-specific tissue regeneration by incorporating bone morphogenetic protein and controlling the shell thickness of silk fibroin/chitosan/nanohydroxyapatite core-shell nanofibrous membranes, ACS Appl. Mater. Interfaces 7 (38) (2015) 21170–21181.

[2] E. Gibon, L.Y. Lu, K. Nathan, S.B. Goodman, Inflammation, ageing, and bone regeneration, J. Orthop. Translat. 10 (2017) 28–35.

[3] M. Pei, J. Seidel, G. Vunjak-Novakovic, L.E. Freed, Growth factors for sequential cellular de- and re-differentiation in tissue engineering, Biochem. Biophys. Res. Commun. 294 (1) (2002) 149–154.

[4] G. Cheng, C. Yin, H. Tu, S. Jiang, Q. Wang, X. Zhou, X. Xing, C. Xie, X. Shi, Y. Du, et al., Controlled co-delivery of growth factors through layer-by-layer assembly of core-shell nanofibers for improving bone regeneration, ACS Nano 13 (6) (2019) 6372–6382.

[5] L. Wu, Y. Gu, L. Liu, J. Tang, J. Mao, K. Xi, Z. Jiang, Y. Zhou, Y. Xu, L. Deng, et al., Hierarchical micro/nanofibrous membranes of sustained releasing VEGF for periosteal regeneration, Biomaterials 227 (2019) 119555.

[6] J. Xue, M. He, Y. Liang, Fabrication and evaluation of electrospun PCL-gelatin micro-/nanofiber membranes for anti-infective GTR implants, J. Mater. Chem. B 2 (2014) 6867–6877.

[7] J. Xue, J. Xie, W. Liu, Y. Xia, Electrospun nanofibers: New concepts, materials, and applications, Acc. Chem. Res. 50 (8) (2017) 1976–1987.

[8] B. Sun, Y. Long, Z. Chen, S. Liu, H. Zhang, J. Zhang, W. Han, Recent advances in flexible and stretchable electronic devices via electrospinning, J. Mater. Chem. C 2 (7) (2014) 1209–1219.

[9] C. Wang, J. Wang, L. Zeng, Z. Qiao, X. Liu, H. Liu, J. Zhang, J. Ding, Fabrication of electrospun polymer nanofibers with diverse morphologies, Molecules 24 (5) (2019) 834–866.

[10] H.S. Yoo, T.G. Kim, T.G. Park, Surface-functionalized electrospun nanofibers for tissue engineering and drug delivery, Adv. Drug Deliv. Rev. 61 (12) (2009) 1033–1042.

[11] J. Zhao, W. Cui, Functional electrospun fibers for local therapy of cancer, Adv. Fiber Mater. 2 (5) (2020) 229–245.

[12] J. Xue, T. Wu, Y. Dai, Y. Xia, Electrospinning and electrospun nanofibers: methods, materials, and applications, Chem. Rev. 119 (8) (2019) 5298–5415.

[13] Y. Dong, Y. Zheng, K. Zhang, Y. Yao, L. Wang, X. Li, J. Yu, B. Ding, Electrospun nanofibrous materials for wound healing, Adv. Fiber Mater. 2 (2020) 212–227.

[14] J. Zeng, L. Yang, Q. Liang, X. Zhang, H. Guan, X. Xu, X. Chen, X. Jing, Influence of the drug compatibility with polymer solution on the release kinetics of electrospun fiber formulation, J. Control. Release 105 (1–2) (2005) 43–51.

[15] K. Ye, H. Kuang, Z. You, Y. Morsi, X. Mo, Electrospun nanofibers for tissue engineering with drug loading and release, Pharmaceutics 11 (4) (2019) 182–198.

[16] N. Bhardwaj, S.C. Kundu, Electrospinning: a fascinating fiber fabrication technique, Biotechnol. Adv. 28 (3) (2010) 325–347.

[17] H.J. Cho, S.K. Perikamana, J.H. Lee, J. Lee, K.M. Lee, C.S. Shin, H. Shin, Effective immobilization of BMP-2 mediated by polydopamine coating on biodegradable nanofibers for enhanced in vivo bone formation, ACS Appl. Mater. Interfaces. 6 (14) (2014) 11225–11235.

[18] C. Wang, M. Wang, Electrospun multicomponent and multifunctional nanofibrous bone tissue engineering scaffolds, J. Mater. Chem. B 5 (7) (2017) 1388–1399.

[19] L. Li, G. Zhou, Y. Wang, G. Yang, S. Ding, S. Zhou, Controlled dual delivery of BMP-2 and dexamethasone by nanoparticle-embedded electrospun nanofibers for the efficient repair of critical-sized rat calvarial defect, Biomaterials 37 (2015) 218–229.

[20] C. Zhu, J. Xue, K.D. Gilroy, D. Huo, S. Shen, Y. Xia, Micropatterned polymer nanorod forests and their use for dual drug loading and regulation of cell adhesion, ACS Appl. Mater. Interfaces. 8 (50) (2016) 34194–34197.

[21] M. Monfared, S. Taghizadeh, A. Zare-Hoseinabadi, S.M. Mousavi, S.A. Hashemi, S. Ranjbar, A.M. Amani, Emerging frontiers in drug release control by core-shell nanofibers: a review, Drug Metab. Rev. 51 (4) (2019) 589–611.

[22] E. Amler, E. Filova, M. Buzgo, E. Prosecka, M. Rampichova, A. Necas, P. Nooeaid, A.R. Boccaccini, Functionalized nanofibers as drug-delivery systems for osteochondral regeneration, Nanomedicine (Lond) 9 (7) (2014) 1083–1094.

[23] J. Wang, M. Windbergs, Controlled dual drug release by coaxial electrospun fibers-impact of the core fluid on drug encapsulation and release, Int. J. Pharm. 556 (2019) 363–371.

[24] G. Kabay, C. Demirci, G. Kaleli Can, A.E. Meydan, B.G. Dasan, M. Mutlu, A comparative study of single-needle and coaxial electrospun amyloid-like protein nanofibers to investigate hydrophilic drug release behavior, Int. J. Biol. Macromol. 114 (2018) 989–997.

[25] X. Shi, Biomedical fibers and nanofibers, Adv. Fiber Mater. 2 (4) (2020) 185.

[26] K. Qiu, C. He, W. Feng, W. Wang, X. Zhou, Z. Yin, L. Chen, H. Wang, X. Mo, Doxorubicin-loaded electrospun poly(l-lactic acid)/mesoporous silica nanoparticles composite nanofibers for potential postsurgical cancer treatment, J. Mater. Chem. B 1 (36) (2013) 4601–4611.

[27] Z. Man, L. Yin, Z. Shao, X. Zhang, X. Hu, J. Zhu, L. Dai, H. Huang, L. Yuan, C. Zhou, et al., The effects of co-delivery of BMSC-affinity peptide and rhTGF-β1 from coaxial electrospun scaffolds on chondrogenic differentiation, Biomaterials 35 (19) (2014) 5250–5260.

[28] C. Hu, W. Cui, Hierarchical structure of electrospun composite fibers for long-term controlled drug release carriers, Adv. Healthc. Mater. 1 (6) (2012) 809–814.

[29] D. Han, S. Sherman, S. Filocamo, A.J. Steckl, Long-term antimicrobial effect of nisin released from electrospun triaxial fiber membranes, Acta Biomater. 53 (2017) 242–249.

[30] D. Yu, X. Li, X. Wang, J. Yang, S.W. Bligh, G.R. Williams, Nanofibers fabricated using triaxial electrospinning as zero order drug delivery systems, ACS Appl. Mater. Interfaces 7 (33) (2015) 18891–18897.

[31] W. Liu, C. Ni, D.B. Chase, J.F. Rabolt, Preparation of multilayer biodegradable nanofibers by triaxial electrospinning, ACS Macro Lett. 2 (6) (2013) 466–468.

[32] Y. Yang, W. Li, D.G. Yu, G. Wang, G.R. Williams, Z. Zhang, Tunable drug release from nanofibers coated with blank cellulose acetate layers fabricated using tri-axial electrospinning, Carbohydr. Polym. 203 (2019) 228–237.

[33] S. Labbaf, H. Ghanbar, E. Stride, M. Edirisinghe, Preparation of multilayered polymeric structures using a novel four-needle coaxial electrohydrodynamic device, Macromol. Rapid Commun. 35 (6) (2014) 618–623.

[34] M. Shin, H. Yoshimoto, J.P. Vacanti, In vivo bone tissue engineering using mesenchymal stem cells on a novel electrospun nanofibrous scaffold, Tissue Eng. 10 (1–2) (2004) 33–41.

[35] A. Sarasam, S.V. Madihally, Characterization of chitosan-polycaprolactone blends for tissue engineering applications, Biomaterials 26 (27) (2005) 5500–5508.

[36] S.H. Huang, T.T. Hsu, T.H. Huang, C.Y. Lin, M.Y. Shie, Fabrication and characterization of polycaprolactone and tricalcium phosphate composites for tissue engineering applications, J. Dent. Sci. 12 (1) (2017) 33–43.

[37] V. Cirillo, V. Guarino, L. Ambrosio, Design of bioactive electrospun scaffolds for bone tissue engineering, J. Appl. Biomater. Funct. Mater. 10 (3) (2012) 223–228.

[38] N. Kathuria, A. Tripathi, K.K. Kar, A. Kumar, Synthesis and characterization of elastic and macroporous chitosan-gelatin cryogels for tissue engineering, Acta Biomater. 5 (1) (2009) 406–418.

[39] J. Xue, R. Shi, Y. Niu, M. Gong, P. Coates, A. Crawford, D. Chen, W. Tian, L. Zhang, Fabrication of drug-loaded anti-infective guided tissue regeneration membrane with adjustable biodegradation property, Colloids Surf. B. Biointerfaces 135 (2015) 846–854.

[40] R. Fu, C. Li, C. Yu, H. Xie, S. Shi, Z. Li, Q. Wang, L. Lu, A novel electrospun membrane based on moxifloxacin hydrochloride/poly(vinyl alcohol)/sodium alginate for antibacterial wound dressings in practical application, Drug Deliv. 23 (3) (2016) 828–839.

[41] P.C. Appelbaum, P.A. Hunter, The fluoroquinolone antibacterials: past, present and future perspectives, Int. J. Antimicrob. Agents 16 (1) (2000) 5–15.

[42] J. Xue, M. He, Y. Niu, H. Liu, A. Crawford, P. Coates, D. Chen, R. Shi, L. Zhang, Preparation and in vivo efficient anti-infection property of GTR/GBR implant made by metronidazole loaded electrospun polycaprolactone nanofiber membrane, Int. J. Pharm. 475 (1–2) (2014) 566–577.

[43] J. Xue, Y. Niu, M. Gong, R. Shi, D. Chen, L. Zhang, Y. Lvov, Electrospun microfiber membranes embedded with drug-loaded clay nanotubes for sustained antimicrobial protection, ACS Nano 9 (2) (2015) 1600–1612.

[44] Z. Zhu, Y. Liu, Y. Xue, X. Cheng, W. Zhao, J. Wang, R. He, Q. Wan, X. Pei, Tazarotene released from aligned electrospun membrane facilitates cutaneous wound healing by promoting angiogenesis, ACS Appl. Mater. Interfaces 11 (39) (2019) 36141–36153.

[45] J. Xue, M. He, H. Liu, Y. Niu, A. Crawford, P.D. Coates, D. Chen, R. Shi, L. Zhang, Drug loaded homogeneous electrospun PCL/gelatin hybrid nanofiber structures for anti-infective tissue regeneration membranes, Biomaterials 35 (34) (2014) 9395–9405.

[46] M. Gong, C. Huang, Y. Huang, G. Li, C. Chi, J. Ye, W. Xie, R. Shi, L. Zhang, Core-sheath micro/nano fiber membrane with antibacterial and osteogenic dual functions as biomimetic artificial periosteum for bone regeneration applications, Nanomedicine 17 (2019) 124–136.

[47] D.W. Hutmacher, Scaffolds in tissue engineering bone and cartilage, Biomaterials 21 (24) (2001) 2529–2543.

[48] B. Zhang, T.M. Filion, A.B. Kutikov, S. Jie, Facile stem cell delivery to bone grafts enabled by smart shape recovery and stiffening of degradable synthetic periosteal membranes, Adv. Funct. Mater. 27 (5) (2016) 1604784.

[49] M. Gong, C. Chi, J. Ye, M. Liao, W. Xie, C. Wu, R. Shi, L. Zhang, Icariin-loaded electrospun PCL/gelatin nanofiber membrane as potential artificial periosteum, Colloids Surf. B. Biointerfaces 170 (2018) 201–209.